JACS
JOURNAL OF THE AMERICAN CHEMICAL SOCIETY
Article
Cite This: J. Am. Chem. Soc. 2019, 141, 14403−14410
pubs.acs.org/JACS

A Wavy Two-Dimensional Covalent Organic Framework from Core-Twisted Polycyclic Aromatic Hydrocarbons

Marta Martínez-Abadía,[†] Craig T. Stoppiello,[‡,§] Karol Strutynski,[∥] Belén Lerma-Berlanga,[⊥] Carlos Martí-Gastaldo,[⊥] Akinori Saeki,[#] Manuel Melle-Franco,*[,∥] Andrei N. Khlobystov,*[,‡,§] and Aurelio Mateo-Alonso*[,†,○]

[†]POLYMAT, University of the Basque Country UPV/EHU, Avenida de Tolosa 72, Donostia-San Sebastian E-20018, Spain
[‡]School of Chemistry, and [§]The Nanoscale and Microscale Research Centre, University of Nottingham, University Park, Nottingham NG7 2RD, United Kingdom
[∥]CICECO - Aveiro Institute of Materials, Department of Chemistry, University of Aveiro, Aveiro 3810-193, Portugal
[⊥]Instituto de Ciencia Molecular, Universidad de Valencia, Paterna 46980, Spain
[#]Department of Applied Chemistry, Graduate School of Engineering, Osaka University, Suita, Osaka 565-0871, Japan
[○]Ikerbasque, Basque Foundation for Science, Bilbao 48013, Spain

Supporting Information

ABSTRACT: A high degree of crystallinity is an essential aspect in two-dimensional covalent organic frameworks, as many properties depend strongly on the structural arrangement of the different layers and their constituents. We introduce herein a new design strategy based on core-twisted polycyclic aromatic hydrocarbon as rigid nodes that give rise to a two-dimensional covalent organic framework with a wavy honeycomb (chairlike) lattice. The concave−convex self-complementarity of the wavy two-dimensional lattice guides the stacking of framework layers into a highly stable and ordered covalent organic framework that allows a full 3D analysis by transmission electron microscopy revealing its chairlike honeycomb facets and aligned mesoporous channels. Remarkably, the waviness of the framework does not disrupt the interlayer $\pi-\pi$ stacking that shows charge transporting properties similar to those of planar covalent organic frameworks. The implementation of core-twisted aromatics as building blocks for covalent organic frameworks brings new possibilities in the design of highly ordered organic materials.

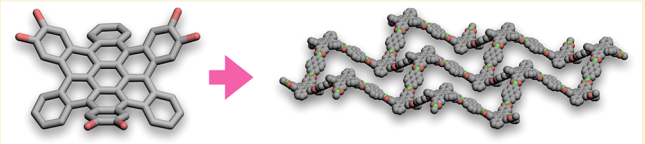

INTRODUCTION

Covalent organic frameworks (COFs) are long-range ordered porous organic structures held together by covalent bonds that have shown a lot of potential as materials for gas separation and storage, liquid filtration and purification, heterogeneous catalysis, sensing, electronics, and energy conversion and storage applications.[1−10] Among these, two-dimensional COFs (2D COFs) are constituted by COF layers that upon packing give rise to organized porous channels and to piled-up organic components from which different adsorbing, catalytic, and electron and exciton transporting properties can emerge, among many others.[11−21]

A high degree of crystallinity is an essential aspect in 2D COFs, as many of the above-mentioned properties depend strongly on the structural arrangement of the different layers and their constituents. Furthermore, a high degree of crystallinity improves the ease of not only the screening and optimization of reaction conditions but also the ability to establish the structure of the resulting 2D COFs. Different approaches have been developed to increase the crystallinity of 2D COFs. These include reactivity- and condition-dependent approaches, such as those based on (i) the reversibility of the bond formation reactions[19] and on (ii) seeded growth,[22] in addition to structure-dependent approaches, such as the introduction of (iii) self-assembling motiffs[23−26] and of (iv) stackable precursors.[27−32]

In particular, the introduction of stackable precursors with distinct shapes, such as bowl-, propeller-, and armchair-shaped precursors,[27−32] relies on their structural self-complementarity that guides the stacking of COF layers during growth. However, current designs of stackable precursors[27−32] involve elements with a high degree of conformational freedom that allow several interconverting conformations that interfere with the stackability of the precursors and of the resulting layers, and, therefore, conformational synchronization during COF formation is required.

We introduce herein a new design strategy that relies on the use of core-twisted polycyclic aromatic hydrocarbons as rigid nonplanar nodes, 2,3,10,11,18,19-hexahydroxy-*cata*-hexabenzocoronene (HBC) (Figure 1). HBC adopts a twisted and rigid structure that is conformationally locked as the result of

Received: July 11, 2019
Published: September 3, 2019

DOI: 10.1021/jacs.9b07383
J. Am. Chem. Soc. 2019, 141, 14403−14410

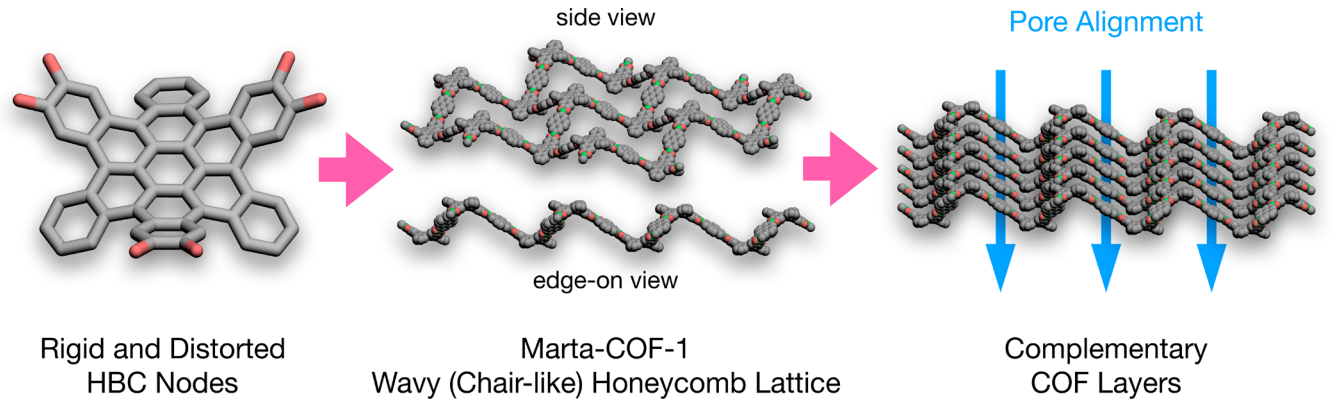

Figure 1. Schematic representation of the rigid and distorted HBC nodes and their incorporation in boronate ester COFs to obtain Marta-COF-1 with a wavy and highly complementary structure that guides the stacking of COF layers.

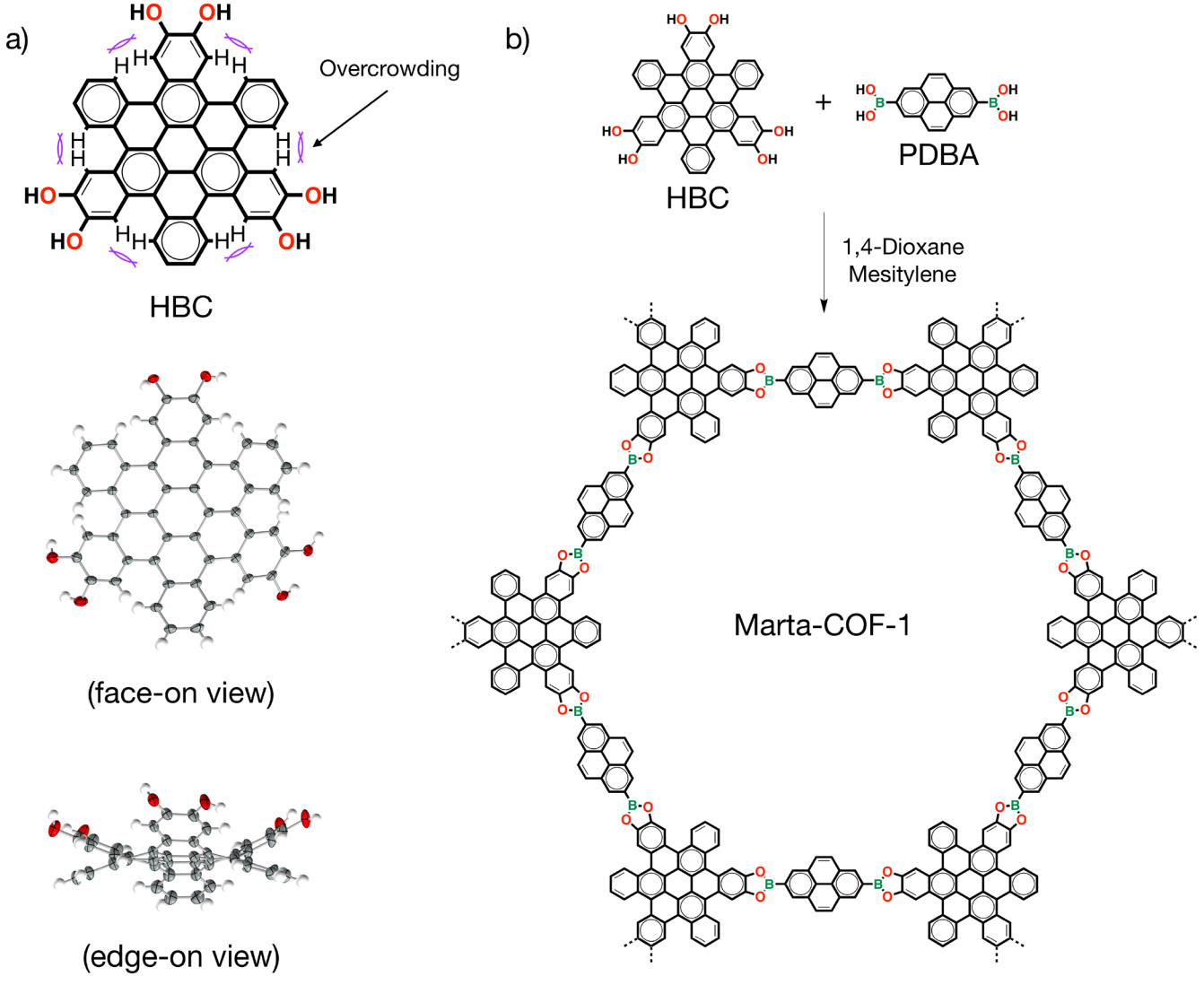

Figure 2. (a) Chemical structure and face-on and edge-on views of the X-ray crystal structure of HBC. (b) Synthesis of Marta-COF-1.

steric congestion between the hydrogens in the peripheral benzene rings (Figures 1 and 2a). The copolymerization of the twisted HBC with pyrene-2,7-diboronic acid (PDBA) produces a highly crystalline 2D COF with a wavy honeycomb (chairlike) lattice (Marta-COF-1, Figure 1).

The concave−convex self-complementarity of the wavy lattice of Marta-COF-1, underpinned by the intrinsic rigidity and the tendency to self-assemble of the HBC nodes, lines up the chairlike mesopores of the individual layers into open channels with a surface area close to the theoretical value. Remarkably, the high stability and crystallinity of Marta-COF-

DOI: 10.1021/jacs.9b07383
J. Am. Chem. Soc. 2019, 141, 14403−14410

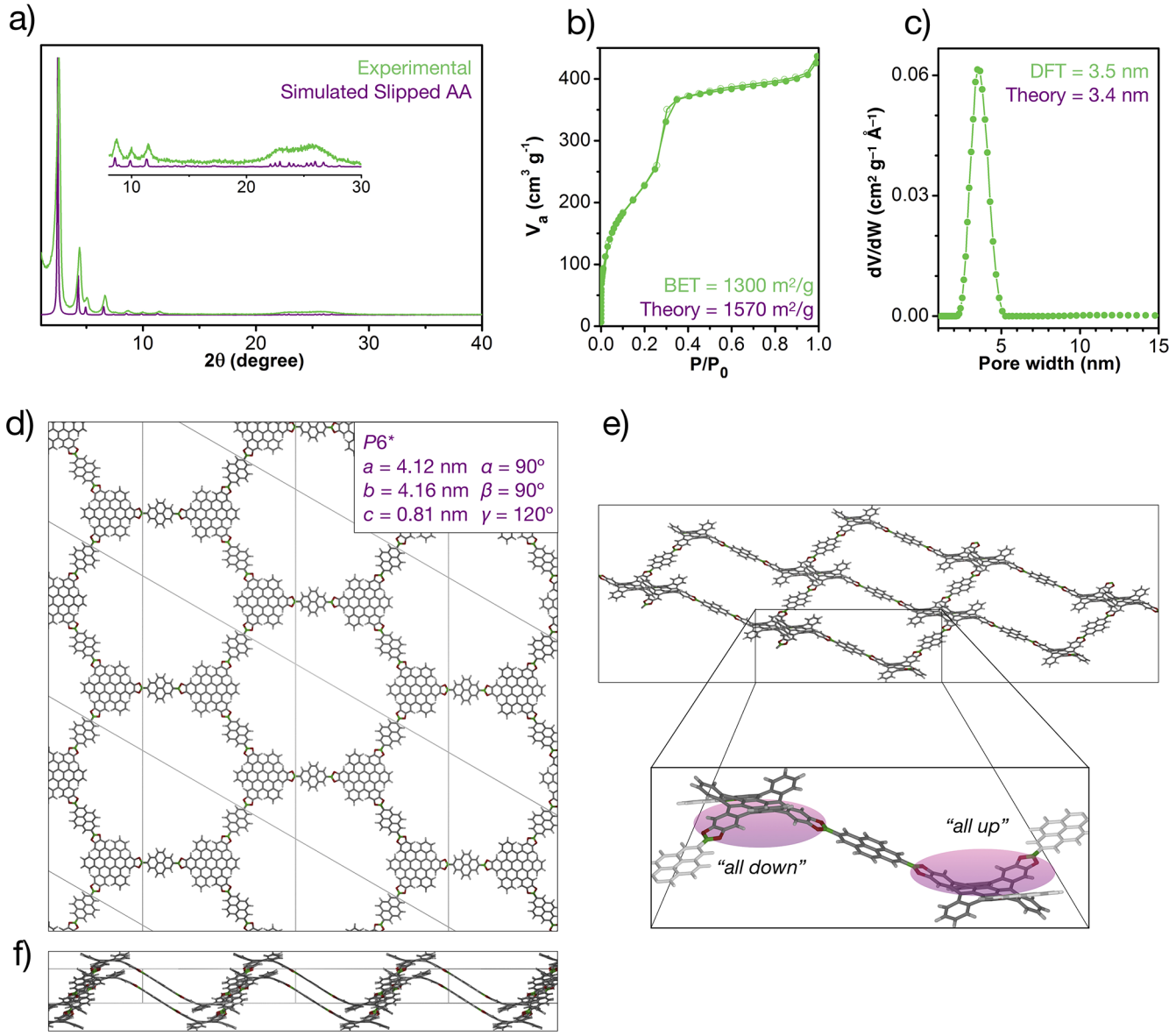

Figure 3. (a) Experimental PXRD pattern and simulated PXRD pattern for the reconstructed crystal structure of Marta-COF-1. (b) Nitrogen adsorption and desorption isotherms at 77 K of Marta-COF-1. (c) DFT pore size distribution of Marta-COF-1. (d) Face-on, (e) lateral, and (f) edge-on views of the reconstructed crystal structure of Marta-COF-1.

1 allow imaging its chairlike honeycomb facets and aligned mesoporous channels by high-resolution transmission electron microscopy (HR-TEM) and TEM tomography, which provide unambiguous visual evidence of the wavy structural features of Marta-COF-1. Furthermore, the waviness of the framework does not disrupt the interlayer $\pi-\pi$ stacking. In consequence, Marta-COF-1 shows charge transporting properties similar to those of the best performing planar 2D COFs.

RESULTS AND DISCUSSION

We selected *cata*-hexabenzocoronene derivatives as nodes because of their nonplanar structure, their structural self-complementarity, and their tendency to self-assemble.[33−37] We focused on the introduction of alternated catechol functionalities in the peripheral rings of *cata*-hexabenzocoronene core so these derivatives can be directly implemented as precursors of boronate ester COFs. HBC was synthesized by ether cleavage of 2,3,10,11,18,19-hexamethoxy-*cata*-hexabenzocoronene[38] in the presence of BBr_3 in a quantitative yield. Single-crystal X-ray diffraction shows that HBC adopts a rigid contorted structure as the result of steric congestion between the hydrogens in the peripheral benzene rings that forces them below and above the plane (Figure 2a and Table S1). This alternated disposition of peripheral benzene rings generates a double-bowl structure that sets all of the catechol groups above the coronene plane. The hexabenzocoronene core does not undergo any conformational change within the temperature range (−30 to 130 °C) required for COF synthesis, as demonstrated by VT-NMR of 2,3,10,11,18,19-hexamethoxy-*cata*-hexabenzocoronene, in which the structure of the ^{1}H NMR signals remains nearly invariable with the increase of temperature and only the typical chemical shifts associated with the temperature change are observed (Figure S1).

Marta-COF-1 was obtained as a yellow solid in a 95% yield by solvothermal condensation of HBC and pyrene-2,7-diboronic acid (PDBA) in a mixture of 1,4-dioxane and

DOI: 10.1021/jacs.9b07383
J. Am. Chem. Soc. 2019, 141, 14403−14410

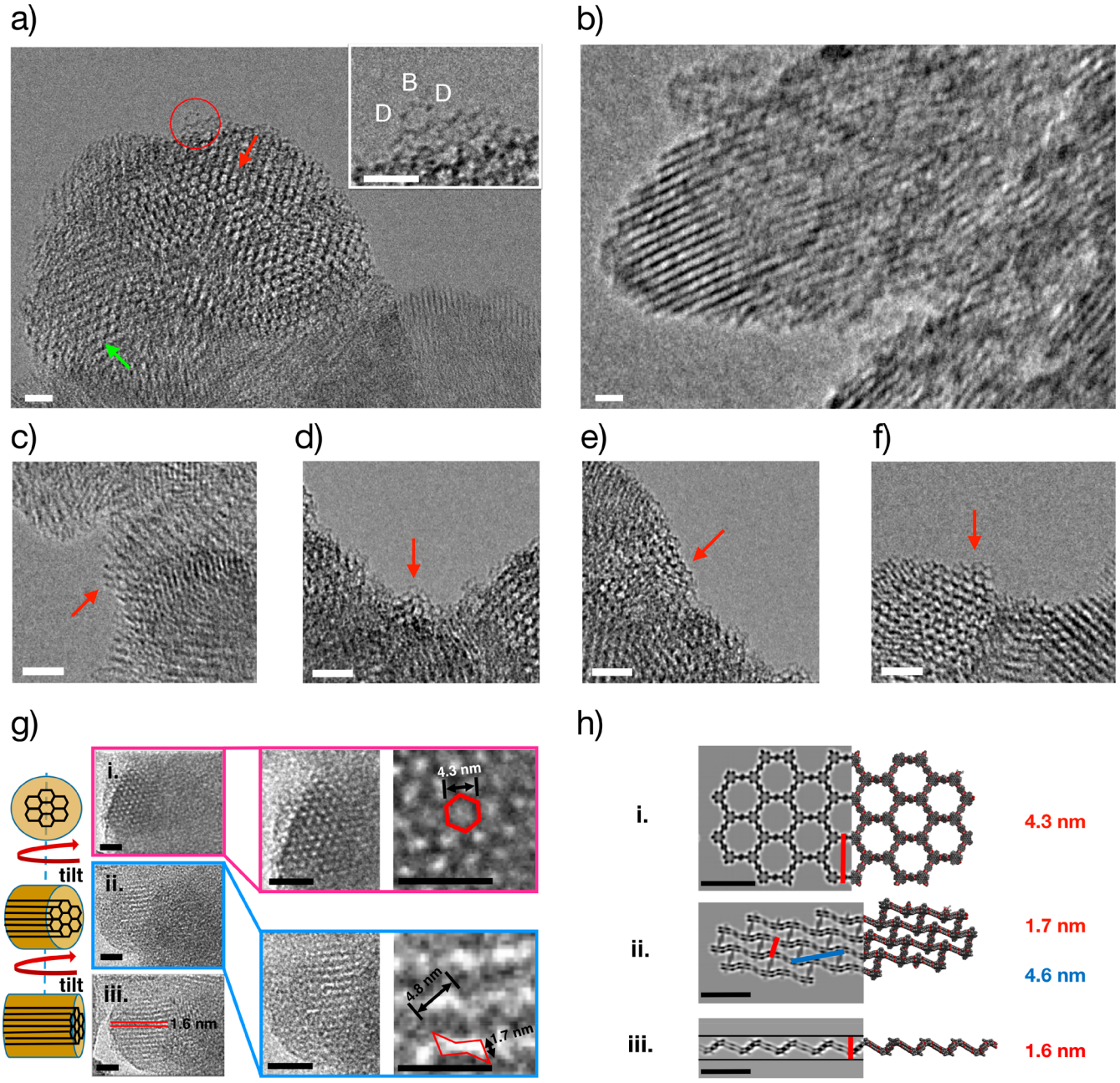

Figure 4. HR-TEM images of highly crystalline domains of Marta-COF-1 on (a) face-on, (b) edge-on, and (c) chairlike configurations, of (d) an individual hexagonal feature, and of (e) zigzag and (f) armchair edges. The scale bars are 10 nm. (g) HR-TEM images showing a Marta-COF-1 particle rotated and imaged over 70° tilt angle within the plane of the page (panels i–iii). The scale bars are 10 nm. Panels (i) and (ii) are magnified. (h) Merged QSTEM HR-TEM simulations (left) with the corresponding geometry optimized models (right) showing the COF in (i) face-on, (ii) chairlike, and (iii) edge-on configurations. The scale bars are 5 nm.

mesitylene (2:1) at 120 °C for 72 h in a sealed prescored ampule (Figure 2b). The successful polymerization of the starting materials was ascertained by FT-IR that shows the appearance of a strong C–O stretching band distinctive for boronate ester five-membered rings at 1337 and 1347 cm^{-1} together with strongly attenuated signals of the hydroxyls of the boronic acid (Figure S2). The solid-state cross-polarization magic angle spinning (CP/MAS) ^{13}C NMR spectrum of Marta-COF-1 (Figure S3) shows the aromatic signals of the hexabenzocoronene and pyrene constituents, while the CP/MAS ^{11}B NMR spectrum (Figure S4) shows a single peak attributed to a single type of boronate ester linkage, both of which are consistent with the structure of Marta-COF-1. Marta-COF-1 shows the same solvent stability as other boronate ester COFs and hydrolyzes in protic solvents such as MeOH and EtOH. The thermal stability was investigated by thermal gravimetric analysis under N_2 (Figure S5), revealing that Marta-COF-1 retained 95% of its mass up to 350 °C.

The PXRD diffractogram of Marta-COF-1 (Figure 3a) shows a large number of resolved reflections at 2.56°, 4.40°, 5.07°, 6.67°, 8.68°, 10.00°, and 11.45°, which correspond to the (100), (2$\bar{1}$0), (020), (120), (2$\bar{4}$0), (400), and (4$\bar{5}$0) Bragg peaks. The presence of these sharp XRD peaks indicates that Marta-COF-1 exhibits a high degree of crystallinity with long-range periodic order. Pawley refinement using a unit cell of a =

DOI: 10.1021/jacs.9b07383
J. Am. Chem. Soc. 2019, 141, 14403–14410

b = 41.5 Å and c = 4.0 Å confirmed the assignment (Figure S6).

The surface areas and pore size distribution of Marta-COF-1 were characterized by nitrogen adsorption measurements at 77 K (Figure 3b and c). Marta-COF-1 exhibits a reversible type IV isotherm with a microporous and mesoporous region. The Brunauer–Emmet–Teller (BET) surface area was calculated to be 1300 $m^2 g^{-1}$ with a pore volume value of 0.677 $cm^3 g^{-1}$. The estimated pore size from the Density Functional Theory (DFT) model is 3.5 nm.

The crystal structure of Marta-COF-1 was reconstructed with the expected slipped AA packing (Figure 3d–f) imposed by the complementary wavy lattice and by the HBC and pyrene constituents from a preoptimized structure using semiempirical Density Functional Theory Tight Binding (DFTB), followed by a final optimization using Density Functional Theory (DFT). The simulations of the slipped AA packing reproduce perfectly the PXRD pattern; meanwhile, the AB packing models show a completely different PXRD pattern (Figure S7).[39] The reconstructed crystal structure reveals the chairlike honeycomb lattice (Figure 3e and f). Such chairlike lattice is the result of the alternated arrangement of HBC nodes with the cathecol groups above the coronene plane (all up) and HBC nodes with the cathecol groups below the coronene plane (all down) (Figure 3f).

In addition, the reconstructed crystal structure exposes how the concave–convex complementarity between layers and the tight layer packing (centroid-to-centroid π-stacking distances are 3.4 Å at the pyrene segments and 3.7 Å at the HBC nodes) generates hexagonal mesoporous channels (Figure 3e and f). The calculated surface area and pore size obtained from the reconstructed crystal structure of Marta-COF-1 are 1570 $m^2 g^{-1}$ and 3.4 nm, respectively. The excellent agreement in the experimental and theoretical values of surface area and pore size (Figure 3b and c) corroborates that Marta-COF-1 is a highly crystalline material.

Field-emission scanning electron microscopy (FE-SEM) and HR-TEM of Marta-COF-1 showed dahlia-like aggregates that extend beyond the micrometer in size (Figures S8 and S9, respectively). Upon closer inspection, the HR-TEM images reveal that Marta-COF-1 crystallizes with domains that extend from tens to hundreds of nanometers. Remarkably, the chairlike honeycomb facets of Marta-COF-1 can be easily observed, which provides direct evidence of the wavy structural features of Marta-COF-1 and also provides additional evidence of the high degree of crystallinity. In some areas, the crystallites are sitting face-on showing the lattice's highly ordered hexagonal mesopores (Figure 4a, red arrow and Figure S10) of 4.3–4.5 nm (pore size ca. 3.5 nm).[40] The mesoporous dimensions observed in HR-TEM are also in agreement with the pore sizes estimated from the N_2 sorption measurements and the reconstructed crystal structure. In other areas, the crystallites are sitting edge-on revealing straight channels that extend across the crystalline domains consistent with the pore size (ca. 3.6 nm) and with the slipped AA packing (Figures 4b and S11). Other areas evidence chairlike features supportive of the chairlike structure of Marta-COF-1 (Figure 4a, green arrow and Figure 4c).

Individual layers of Marta-COF-1 can be distinguished at the edges (Figure 4a, circled area and Figure 4d), which allow investigating the structure of the unpacked honeycomb lattice lying in the vacuum. A closer inspection of such edges (inset of Figure 4a) reveals alternating bright (B) and dark (D) features in the nodes of each hexagon, which are consistent with the chairlike honeycomb lattice dimensions and with the estimated 6.6 Å height difference between the adjacent nodes estimated for an individual layer (Figure S12). Such alternating bright and dark features are ubiquitous to edges of COF particles when viewed face-on (Figure 4d–f).

The high crystallinity also allows identifying both zigzag (Figure 4e) and armchair edges (Figure 4f). The hexagonal structures at the edges show a slightly larger hexagon diameter, ca. 4.7 nm (pore size ca. 3.7 nm), than those observed within the bulk of the structure, ca. 4.5 nm (pore size ca. 3.5 nm). This is confirmed by the line profiles from crystalline features in both the bulk structure and the edge that show smaller pore diameter in the bulk domains (Figure S13). These edge-bulk pore size differences can be rationalized in terms of the higher flexibility of the COF monolayers lying in the vacuum that gives rise to structures with a larger pore size in comparison to those packed in the bulk. This interpretation is also in agreement with the simulations on a free-standing Marta-COF-1 layer that shows larger diameters than those in a condensed phase (Figure S12).

TEM tomography, a process of sequential imaging and tilting of a particle, has been previously reported to be an excellent method to elucidate the internal structure of COFs and less crystalline conjugated microporous polymers;[41] however, this technique is limited by the stability of the samples. Thanks to the high stability of Marta-COF-1, it was possible performing HR-TEM tilt series imaging experiments of individual crystallites over 70° (Figures 4g and S14). The images confirm that the observed hexagons, channel cross sections, and chairlike features are not only consistent with the dimensions and with the chairlike honeycomb structure of Marta-COF-1 but also interrelated to each other.[42] As a matter of fact, while the first frame of the tilt series shows hexagons corresponding to a view down the channels (Figure 4g, i), the tilting of the particle eventually shows wavy features and a side-view of the COF channel in a chairlike configuration (Figure 4g, ii). Additional tilting reveals how the hexagons transform into the previously observed channels (Figure 4g, iii). Such TEM image–structure correlations have been further confirmed by QSTEM[43] HR-TEM simulations of the geometry-optimized models of a bilayer of Marta-COF-1 in face-on (Figure 4h, i), chairlike (Figure 4h, ii), and edge-on (Figure 4h, iii) that reproduced the features, electron density profiles, and distances observed experimentally (Figure 4g and Figure S14).

In planar 2D COFs, the π-stacking between layers can open channels for charge transport across the columns obtained from the layers' π-stacked constituents. An open question is if the wavy structure of Marta-COF-1 could interfere with the charge transporting properties, because COFs with efficient charge transporting channels are obtained by the stacking of planar 2D COF. To assess the charge transporting properties of Marta-COF-1, we used the flash-photolysis time-resolved microwave conductivity (FP-TRMC) technique,[44] which has emerged as a standard to study the charge transporting properties of COFs. This is because interfacing COFs with electrodes is still a challenging task and FP-TRMC is an electrode-less technique that can be used to measure directly powders and films. FP-TRMC estimates the pseudophotoconductivity ($\varphi\Sigma\mu$) that provides an estimation of the intrinsic charge carrier mobility of the material. The $\varphi\Sigma\mu$ value is the product of the quantum yield (φ) and the sum of the charge carrier mobilities ($\Sigma\mu$). For comparison, samples of crystalline

DOI: 10.1021/jacs.9b07383
J. Am. Chem. Soc. 2019, 141, 14403–14410

powders Marta-COF-1 and of thin films of crystalline powders of Marta-COF-1 dispersed in polytriarylamine were studied and compared. The samples of Marta-COF-1 dispersed in a polytriarylamine ($\varphi\Sigma\mu_{max}$ = 0.9 × 10^{-4} cm^2 V^{-1} s^{-1}) showed slightly higher $\varphi\Sigma\mu_{max}$ values (Figure 5), but in the same order

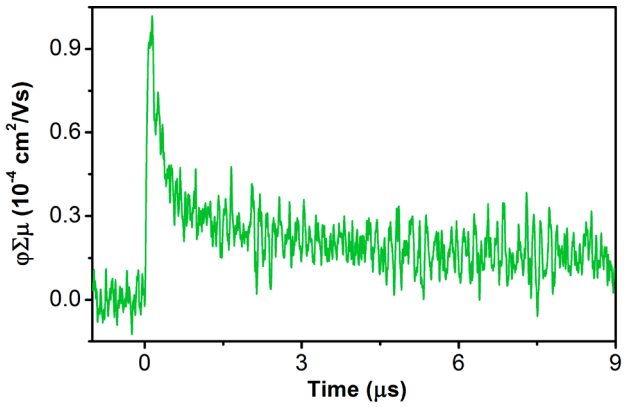

Figure 5. $\varphi\Sigma\mu$ of a thin film of Marta-COF-1 measured by FP-TRMC.

of magnitude as the powders of Marta-COF-1 ($\varphi\Sigma\mu_{max}$ = 0.6 × 10^{-4} cm^2 V^{-1} s^{-1}). These nearly invariable $\varphi\Sigma\mu$ values for Marta-COF-1 are on the same order of magnitude as those observed in the best performing planar 2D COFs[45−53] (with $\varphi\Sigma\mu$ values between 10^{-5} and 10^{-4} cm^2 V^{-1} s^{-1}). This is consistent with the intimate π-stacking distances (3.4 Å at the pyrene segments and 3.7 Å at the HBC nodes) revealed by the reconstructed crystal structure that show how the framework's waviness does not interfere with charge transport across the layers.

CONCLUSIONS

In summary, we have developed and implemented a design strategy for the synthesis of nonplanar 2D COF on the basis of the use of core-twisted polycyclic aromatic hydrocarbons as nodes. The rigid nonplanar conformation of HBC expresses a 2D chairlike honeycomb lattice as the result of the alternated arrangement of HBC nodes with the cathecol groups facing above the coronene plane and HBC nodes with the cathecol groups below the coronene plane across the lattice. The structural self-complementarity of the twisted nodes and of the wavy lattice favors a slipped AA packing of the layers that line up the hexagonal chairlike mesopores of the individual layers into open channels with a surface area (1300 m^2/g) and pore size (3.5 nm) close to the theoretically predicted values (1587 m^2/g and 3.4 nm, respectively) that evidence that Marta-COF-1 is a highly crystalline material. The high stability and crystallinity of Marta-COF-1 have allowed an extraordinary level of characterization by HR-TEM. For instance, HR-TEM images show chairlike honeycomb facets and aligned mesoporous channels consistent with the experimental and predicted dimensions and packing, and also it has been possible to identify both free-standing individual chairlike hexagons, and zigzag and armchair edges. Furthermore, TEM tomography evidences how the observed hexagons, channel cross sections, and chairlike features of Marta-COF-1 are interrelated to each other. In addition, Marta-COF-1 exhibits $\varphi\Sigma\mu$ values similar to those of 2D COFs with high charge carrier mobilities because the wavy structure of the lattice does not interfere with the interlayer π-stacking. The implementation of core-twisted aromatics as COF precursors brings new possibilities in the design of highly crystalline 2D and 3D COFs with new architectures and properties.

ASSOCIATED CONTENT

Supporting Information

The Supporting Information is available free of charge on the ACS Publications website at DOI: 10.1021/jacs.9b07383.

Full synthesis and characterization of Marta-COF-1 (PDF)

X-ray structure of HBC (CIF)

AUTHOR INFORMATION

Corresponding Authors

*manuelmelle.research@gmail.com

*andrei.khlobystov@nottingham.ac.uk

*amateo@polymat.eu

ORCID

Karol Strutynski: 0000-0001-8733-9012

Carlos Martí-Gastaldo: 0000-0003-3203-0047

Akinori Saeki: 0000-0001-7429-2200

Manuel Melle-Franco: 0000-0003-1929-0477

Andrei N. Khlobystov: 0000-0001-7738-4098

Aurelio Mateo-Alonso: 0000-0002-5316-2594

Notes

The authors declare no competing financial interest.

ACKNOWLEDGMENTS

M.M.-A. and A.M.-A. acknowledge support of the Basque Science Foundation for Science (Ikerbasque), POLYMAT, the University of the Basque Country (Grupo de Investigación GIU17/054 and SGIker), Diputación Foral de Guipúzcoa (OF215/2016(ES)), Gobierno Vasco (BERC program), and Gobierno de España (Ministerio de Economia y Competitividad CTQ2016-77970-R). M.M.-F. acknowledges support from the Portuguese Foundation for Science and Technology (FCT), under the projects PTDC/FIS-NAN/4662/2014, IF/00894/2015, and FCT ref. UID/CTM/50011/2019 for CICECO - Aveiro Institute of Materials. This project has received funding from the European Union's Horizon 2020 research and innovation programme under grant agreement no. 664878. This project has received funding from the European Research Council (ERC) under the European Union's Horizon 2020 research and innovation programme (grant agreement nos. 722951 and 714122).

REFERENCES

(1) Davis, M. E. Ordered porous materials for emerging applications. *Nature* **2002**, *417*, 813.

(2) Rowsell, J. L. C.; Yaghi, O. M. Metal−organic frameworks: a new class of porous materials. *Microporous Mesoporous Mater.* **2004**, *73* (1), 3−14.

(3) Das, S.; Heasman, P.; Ben, T.; Qiu, S. Porous Organic Materials: Strategic Design and Structure−Function Correlation. *Chem. Rev.* **2017**, *117* (3), 1515−1563.

(4) Zhou, J.; Wang, B. Emerging crystalline porous materials as a multifunctional platform for electrochemical energy storage. *Chem. Soc. Rev.* **2017**, *46* (22), 6927−6945.

(5) Xie, X.-C.; Huang, K.-J.; Wu, X. Metal-organic framework derived hollow materials for electrochemical energy storage. *J. Mater. Chem. A* **2018**, *6* (16), 6754−6771.

(6) Ahmed, D. S.; El-Hiti, G. A.; Yousif, E.; Ali, A. A.; Hameed, A. S. Design and synthesis of porous polymeric materials and their applications in gas capture and storage: a review. *J. Polym. Res.* **2018**, *25* (3), 75.
(7) Xiang, Z.; Yanxiang, W.; Dong Sheng, L.; Xianhui, B.; Pingyun, F. Metal−Organic Frameworks for Separation. *Adv. Mater.* **2018**, *0* (0), 1705189.
(8) Benzigar, M. R.; Talapaneni, S. N.; Joseph, S.; Ramadass, K.; Singh, G.; Scaranto, J.; Ravon, U.; Al-Bahily, K.; Vinu, A. Recent advances in functionalized micro and mesoporous carbon materials: synthesis and applications. *Chem. Soc. Rev.* **2018**, *47* (8), 2680−2721.
(9) Shuai, Y.; Liang, F.; Kecheng, W.; Jiandong, P.; Matheiu, B.; Christina, L.; Yujia, S.; Junsheng, Q.; Xinyu, Y.; Peng, Z.; Qi, W.; Lanfang, Z.; Yingmu, Z.; Liangliang, Z.; Yu, F.; Jialuo, L.; Hong-Cai, Z. Stable Metal−Organic Frameworks: Design, Synthesis, and Applications. *Adv. Mater.* **2018**, *0* (0), 1704303.
(10) Ma, T.; Kapustin, E. A.; Yin, S. X.; Liang, L.; Zhou, Z.; Niu, J.; Li, L.-H.; Wang, Y.; Su, J.; Li, J.; Wang, X.; Wang, W. D.; Wang, W.; Sun, J.; Yaghi, O. M. Single-crystal x-ray diffraction structures of covalent organic frameworks. *Science* **2018**, *361* (6397), 48−52.
(11) Côté, A. P.; Benin, A. I.; Ockwig, N. W.; O'Keeffe, M.; Matzger, A. J.; Yaghi, O. M. Porous, Crystalline, Covalent Organic Frameworks. *Science* **2005**, *310* (5751), 1166−1170.
(12) Ding, S.-Y.; Wang, W. Covalent organic frameworks (COFs): from design to applications. *Chem. Soc. Rev.* **2013**, *42* (2), 548−568.
(13) Colson, J. W.; Dichtel, W. R. Rationally synthesized two-dimensional polymers. *Nat. Chem.* **2013**, *5*, 453.
(14) Waller, P. J.; Gándara, F.; Yaghi, O. M. Chemistry of Covalent Organic Frameworks. *Acc. Chem. Res.* **2015**, *48* (12), 3053−3063.
(15) DeBlase, C. R.; Dichtel, W. R. Moving Beyond Boron: The Emergence of New Linkage Chemistries in Covalent Organic Frameworks. *Macromolecules* **2016**, *49* (15), 5297−5305.
(16) Jiang, J.; Zhao, Y.; Yaghi, O. M. Covalent Chemistry beyond Molecules. *J. Am. Chem. Soc.* **2016**, *138* (10), 3255−3265.
(17) Alahakoon, S. B.; Thompson, C. M.; Occhialini, G.; Smaldone, R. A. Design Principles for Covalent Organic Frameworks in Energy Storage Applications. *ChemSusChem* **2017**, *10* (10), 2116−2129.
(18) Bisbey, R. P.; Dichtel, W. R. Covalent Organic Frameworks as a Platform for Multidimensional Polymerization. *ACS Cent. Sci.* **2017**, *3* (6), 533−543.
(19) Diercks, C. S.; Yaghi, O. M. The atom, the molecule, and the covalent organic framework. *Science* **2017**, *355* (6328), eaal1585.
(20) Beuerle, F.; Gole, B. Covalent Organic Frameworks and Cage Compounds: Design and Applications of Polymeric and Discrete Organic Scaffolds. *Angew. Chem., Int. Ed.* **2018**, *57* (18), 4850−4878.
(21) Chun-Yu, L.; Detao, Z.; Zhenghang, Z.; Zhenhai, X. Covalent Organic Framework Electrocatalysts for Clean Energy Conversion. *Adv. Mater.* **2018**, *30* (5), 1703646.
(22) Evans, A. M.; Parent, L. R.; Flanders, N. C.; Bisbey, R. P.; Vitaku, E.; Kirschner, M. S.; Schaller, R. D.; Chen, L. X.; Gianneschi, N. C.; Dichtel, W. R. Seeded growth of single-crystal two-dimensional covalent organic frameworks. *Science* **2018**, *361* (6397), 52−57.
(23) Chen, X.; Addicoat, M.; Irle, S.; Nagai, A.; Jiang, D. Control of Crystallinity and Porosity of Covalent Organic Frameworks by Managing Interlayer Interactions Based on Self-Complementary π-Electronic Force. *J. Am. Chem. Soc.* **2013**, *135* (2), 546−549.
(24) Chen, X.; Addicoat, M.; Jin, E.; Zhai, L.; Xu, H.; Huang, N.; Guo, Z.; Liu, L.; Irle, S.; Jiang, D. Locking Covalent Organic Frameworks with Hydrogen Bonds: General and Remarkable Effects on Crystalline Structure, Physical Properties, and Photochemical Activity. *J. Am. Chem. Soc.* **2015**, *137* (9), 3241−3247.
(25) Xu, H.; Gao, J.; Jiang, D. Stable, crystalline, porous, covalent organic frameworks as a platform for chiral organocatalysts. *Nat. Chem.* **2015**, *7*, 905.
(26) Salonen, L. M.; Medina, D. D.; Carbo-Argibay, E.; Goesten, M. G.; Mafra, L.; Guldris, N.; Rotter, J. M.; Stroppa, D. G.; Rodriguez-Abreu, C. A supramolecular strategy based on molecular dipole moments for high-quality covalent organic frameworks. *Chem. Commun.* **2016**, *52* (51), 7986−7989.
(27) Yu, J.-T.; Chen, Z.; Sun, J.; Huang, Z.-T.; Zheng, Q.-Y. Cyclotricatechylene based porous crystalline material: Synthesis and applications in gas storage. *J. Mater. Chem.* **2012**, *22* (12), 5369−5373.
(28) Ascherl, L.; Sick, T.; Margraf, J. T.; Lapidus, S. H.; Calik, M.; Hettstedt, C.; Karaghiosoff, K.; Döblinger, M.; Clark, T.; Chapman, K. W.; Auras, F.; Bein, T. Molecular docking sites designed for the generation of highly crystalline covalent organic frameworks. *Nat. Chem.* **2016**, *8*, 310.
(29) Dalapati, S.; Jin, E.; Addicoat, M.; Heine, T.; Jiang, D. Highly Emissive Covalent Organic Frameworks. *J. Am. Chem. Soc.* **2016**, *138* (18), 5797−5800.
(30) Auras, F.; Ascherl, L.; Hakimioun, A. H.; Margraf, J. T.; Hanusch, F. C.; Reuter, S.; Bessinger, D.; Döblinger, M.; Hettstedt, C.; Karaghiosoff, K.; Herbert, S.; Knochel, P.; Clark, T.; Bein, T. Synchronized Offset Stacking: A Concept for Growing Large-Domain and Highly Crystalline 2D Covalent Organic Frameworks. *J. Am. Chem. Soc.* **2016**, *138* (51), 16703−16710.
(31) Belen, M. A.; Diego, C.-L.; Iñigo, P.-M.; Giovanni, V.; Alessandro, B.; Jan, P.; Karol, S.; Steven, D. F.; Francesco, P.; Mario, M.; N, K. A.; Manuel, M.-F.; Aurelio, M.-A. Twisted Aromatic Frameworks: Readily Exfoliable and Solution-Processable Two-Dimensional Conjugated Microporous Polymers. *Angew. Chem., Int. Ed.* **2017**, *56* (24), 6946−6951.
(32) Thompson, C. M.; Occhialini, G.; McCandless, G. T.; Alahakoon, S. B.; Cameron, V.; Nielsen, S. O.; Smaldone, R. A. Computational and Experimental Studies on the Effects of Monomer Planarity on Covalent Organic Framework Formation. *J. Am. Chem. Soc.* **2017**, *139* (30), 10506−10513.
(33) Sepulveda, D.; Guan, Y.; Rangel, U.; Wheeler, S. E. Stacked homodimers of substituted contorted hexabenzocoronenes and their complexes with C60 fullerene. *Org. Biomol. Chem.* **2017**, *15* (28), 6042−6049.
(34) Guan, Y.; Jones, M. L.; Miller, A. E.; Wheeler, S. E. Conformational behavior and stacking interactions of contorted polycyclic aromatics. *Phys. Chem. Chem. Phys.* **2017**, *19* (28), 18186−18193.
(35) Shengxiong, X.; Matthew, M.; Qian, M.; Sébastien, S.; Keliang, P.; L, S. M.; Colin, N. Molecular Wires from Contorted Aromatic Compounds. *Angew. Chem., Int. Ed.* **2005**, *44* (45), 7390−7394.
(36) Guo, X.; Xiao, S.; Myers, M.; Miao, Q.; Steigerwald, M. L.; Nuckolls, C. Photoresponsive nanoscale columnar transistors. *Proc. Natl. Acad. Sci. U. S. A.* **2009**, *106* (3), 691−696.
(37) Chiu, C.-Y.; Kim, B.; Gorodetsky, A. A.; Sattler, W.; Wei, S.; Sattler, A.; Steigerwald, M.; Nuckolls, C. Shape-shifting in contorted dibenzotetrathienocoronenes. *Chem. Sci.* **2011**, *2* (8), 1480−1486.
(38) Zhang, Q.; Peng, H.; Zhang, G.; Lu, Q.; Chang, J.; Dong, Y.; Shi, X.; Wei, J. Facile Bottom-Up Synthesis of Coronene-based 3-Fold Symmetrical and Highly Substituted Nanographenes from Simple Aromatics. *J. Am. Chem. Soc.* **2014**, *136* (13), 5057−5064.
(39) Computed binding energies between layers per heavy atom (Table S2) show that the slipped AA packing configuration (−0.893 kcal/mol) is indeed more thermodynamically stable than the slipped AB packing configuration (−0.427 kcal/mol).
(40) TEM measures accurate distances from the centroid of the pyrene group in the edge of a hexagonal pore to the centroid of the pyrene group in the opposite edge. Therefore, the measured mesopore diameters do not include the width of the pyrene group or C−H bonds, and appear slightly larger than physical pore diameter. The estimated pore sizes are given as a reference.
(41) Stoppiello, C. T.; Isla, H.; Martínez-Abadía, M.; Fay, M. W.; Parmenter, C. D. J.; Roe, M. J.; Lerma-Berlanga, B.; Martí-Gastaldo, C.; Mateo-Alonso, A.; Khlobystov, A. N. Three dimensional nanoscale analysis reveals aperiodic mesopores in a covalent organic framework and conjugated microporous polymer. *Nanoscale* **2019**, *11* (6), 2848−2854.
(42) The resolution of the TEM topography measurements is lower due to the image being of lower magnification and digitally expanded,

DOI: 10.1021/jacs.9b07383
J. Am. Chem. Soc. 2019, 141, 14403−14410

which had to be the case because of the large size of the particles tilted.
(43) Koch, C. Determination of core structure periodicity and point defect density along dislocations. Ph.D. dissertation, 2002.
(44) Saeki, A.; Koizumi, Y.; Aida, T.; Seki, S. Comprehensive Approach to Intrinsic Charge Carrier Mobility in Conjugated Organic Molecules, Macromolecules, and Supramolecular Architectures. *Acc. Chem. Res.* **2012**, *45* (8), 1193−1202.
(45) Dalapati, S.; Addicoat, M.; Jin, S.; Sakurai, T.; Gao, J.; Xu, H.; Irle, S.; Seki, S.; Jiang, D. Rational design of crystalline supermicroporous covalent organic frameworks with triangular topologies. *Nat. Commun.* **2015**, *6*, 7786.
(46) Ding, H.; Li, Y.; Hu, H.; Sun, Y.; Wang, J.; Wang, C.; Wang, C.; Zhang, G.; Wang, B.; Xu, W.; Zhang, D. A Tetrathiafulvalene-Based Electroactive Covalent Organic Framework. *Chem. - Eur. J.* **2014**, *20* (45), 14614−14618.
(47) Jin, S.; Sakurai, T.; Kowalczyk, T.; Dalapati, S.; Xu, F.; Wei, H.; Chen, X.; Gao, J.; Seki, S.; Irle, S.; Jiang, D. Two-Dimensional Tetrathiafulvalene Covalent Organic Frameworks: Towards Latticed Conductive Organic Salts. *Chem. - Eur. J.* **2014**, *20* (45), 14608−14613.
(48) Feng, X.; Chen, L.; Honsho, Y.; Saengsawang, O.; Liu, L.; Wang, L.; Saeki, A.; Irle, S.; Seki, S.; Dong, Y.; Jiang, D. An Ambipolar Conducting Covalent Organic Framework with Self-Sorted and Periodic Electron Donor-Acceptor Ordering. *Adv. Mater.* **2012**, *24* (22), 3026−3031.
(49) Feng, X.; Liu, L.; Honsho, Y.; Saeki, A.; Seki, S.; Irle, S.; Dong, Y.; Nagai, A.; Jiang, D. High-Rate Charge-Carrier Transport in Porphyrin Covalent Organic Frameworks: Switching from Hole to Electron to Ambipolar Conduction. *Angew. Chem., Int. Ed.* **2012**, *51* (11), 2618−2622.
(50) Ding, X.; Feng, X.; Saeki, A.; Seki, S.; Nagai, A.; Jiang, D. Conducting metallophthalocyanine 2D covalent organic frameworks: the role of central metals in controlling π-electronic functions. *Chem. Commun.* **2012**, *48* (71), 8952−8954.
(51) Wan, S.; Gándara, F.; Asano, A.; Furukawa, H.; Saeki, A.; Dey, S. K.; Liao, L.; Ambrogio, M. W.; Botros, Y. Y.; Duan, X.; Seki, S.; Stoddart, J. F.; Yaghi, O. M. Covalent Organic Frameworks with High Charge Carrier Mobility. *Chem. Mater.* **2011**, *23* (18), 4094−4097.
(52) Ding, X.; Guo, J.; Feng, X.; Honsho, Y.; Guo, J.; Seki, S.; Maitarad, P.; Saeki, A.; Nagase, S.; Jiang, D. Synthesis of Metallophthalocyanine Covalent Organic Frameworks That Exhibit High Carrier Mobility and Photoconductivity. *Angew. Chem., Int. Ed.* **2011**, *50* (6), 1289−1293.
(53) Ding, X.; Chen, L.; Honsho, Y.; Feng, X.; Saengsawang, O.; Guo, J.; Saeki, A.; Seki, S.; Irle, S.; Nagase, S.; Parasuk, V.; Jiang, D. An n-Channel Two-Dimensional Covalent Organic Framework. *J. Am. Chem. Soc.* **2011**, *133* (37), 14510−14513.

DOI: 10.1021/jacs.9b07383
J. Am. Chem. Soc. 2019, 141, 14403−14410